Structure of the isomeric states in ^{123,125}Sb

D. S. Judson,[1] A. M. Bruce,[1,*] T. Kibédi,[2] G. D. Dracoulis,[2] A. P. Byrne,[2,3] G. J. Lane,[2] K. H. Maier,[2] C.-B. Moon,[4] P. Nieminen,[2] J. N. Orce,[1,†] and M. J. Taylor[1,‡]

[1]*School of Engineering, University of Brighton, Brighton BN2 4GJ, United Kingdom*
[2]*Department of Nuclear Physics, Australian National University, Canberra ACT 0200, Australia*
[3]*Department of Physics, The Faculties, Australian National University, Canberra ACT 0200, Australia*
[4]*Department of Display Engineering, Hoseo University, Chung-Nam 336-795, Korea*

(Received 28 August 2007; published 5 November 2007)

Excited states in ^{123,125}Sb have been studied following the ^{122,124}Sn(^{7}Li,α2n)^{123,125}Sb reactions at beam energies of 35 and 37 MeV, respectively. Conversion coefficients for transitions depopulating isomeric states in ^{125}Sb have been measured using an electron spectrometer. This has allowed firm J^{π} assignments to be made and enabled the structure of the isomeric states to be compared with those in $^{121,127-131}$Sb and in the neighboring even-A tin isotopes. The half-lives of the $J^{\pi} = \frac{23}{2}^{+}$ isomeric states in ^{123}Sb and ^{125}Sb have been measured to be 66(4) μs and 272(16) ns, respectively. The half-lives of the $J^{\pi} = \frac{19}{2}^{+}$, $\frac{19}{2}^{-}$, and $\frac{15}{2}^{-}$ states in ^{125}Sb have been measured as 31(2) ns, 28.0(7) μs, and 4.1(2) μs, respectively. The transition probabilities for the transitions depopulating these states are compared with those in $^{121,127-131}$Sb and with the results of shell-model calculations using the Oxbash code and the SN100PN interaction in a restricted model space.

DOI: 10.1103/PhysRevC.76.054306 PACS number(s): 21.10.Tg, 23.20.Lv, 27.60.+j

I. INTRODUCTION

Isomeric $J^{\pi} = \frac{23}{2}^{+}$, $\frac{19}{2}^{-}$, and $\frac{15}{2}^{-}$ states have previously been observed in odd-mass antimony nuclei and have been interpreted [1] as the odd $g_{\frac{7}{2}}$ proton coupled to known isomeric $10^{+}, 7^{-}$, and 5^{-} states in the $^{(A-1)}$Sn core, respectively, based on the energy systematics. Figure 1 shows the energy systematics of these states in $^{121-131}$Sb in comparison with the even-A tin isotopes and indeed a clear correlation is observed. A more stringent test of any comparison requires analysis of transition probabilities. The half-lives of isomeric states in $^{127-131}$Sb are known from measurements of the β decay of $^{127-131}$Sn [1–3] and, for ^{121,123}Sb, from the results of fission fragment experiments [4,5]. The values for ^{125}Sb were measured by [4,6–8] but have large error bars associated with them. In addition, the J^{π} values were uncertain.

Previous work on ^{125}Sb by Liu *et al.* [7,8] reported on the ^{124}Sn(^{7}Li,α2n)^{125}Sb reaction and proposed the existence of three isomeric states: (i) a $(\frac{15}{2}^{-})$ state at 1970 keV with a half-life between 70 and 600 ns, (ii) a $(\frac{19}{2}^{-})$ state at 2110 keV with a lower limit on the half-life given as 2 ms in Ref. [7] and 2 μs in Ref. [8], and (iii) a $(\frac{23}{2}^{+})$ state at 2471 keV with a half-life between 40 and 200 ns. A subsequent study by Porquet *et al.* [4] used the EUROBALL III and IV detectors to study fission fragments induced by heavy-ion reactions but only observed one isomeric state, at 2470 keV, for which they measured a half-life of 155(20) ns and assigned a J^{π} value of $\frac{19}{2}^{-}$. This is not consistent with the $J^{\pi} = \frac{23}{2}^{+}$ assignment made by Liu *et al.* [7,8]. Porquet *et al.* [4] also identified a $J^{\pi} = (\frac{19}{2}^{-})$ isomeric state in ^{123}Sb at an excitation energy of 2237 keV for which a half-life of 110(10) ns was measured. The current article reports the results of experiments aimed at pinning down the J^{π} values of states in ^{125}Sb and measuring the half-lives of isomeric states in ^{123,125}Sb.

II. EXPERIMENTAL PROCEDURE

Excited states in ^{125}Sb were populated using the ^{124}Sn(^{7}Li,α2n)^{125}Sb incomplete fusion reaction. The beam was provided by the 14UD Pelletron Tandem accelerator at the Australian National University (ANU) and the Super-E electron spectrometer [10,11] was used in conjunction with a single germanium detector to measure electron-conversion coefficients and half-lives. In this case a beam energy of 37 MeV was used and the ^{124}Sn target was 1.5 mg/cm^2 thick. Two different beam profiles were used: (i) 2 ns pulses separated by 1.7 μs and (ii) 2.7 μs pulses separated by 85.6 μs. A prompt veto of 2.8 μs was applied in the latter case so that only delayed transitions were recorded. γ-ray and electron energies were recorded along with their time measured with respect to the rf pulse train. These data were used to construct two sets (one for each beam profile) of time-electron and time-γ matrices that contained the energy on one axis and the time on the other.

An experiment to measure the half-lives of long lived ($T_{1/2} > 2$ μs) states in ^{123}Sb was performed using the ^{122}Sn(^{7}Li,α2n)^{123}Sb reaction at a beam energy of 35 MeV. The target was 3.5 mg/cm^2 thick and a beam pulsing profile of 21.4 μs on/428 μs off was used with a prompt veto of 21.7 μs. γ rays were detected in the CAESAR germanium detector array [12], augmented by three Compton suppressed germanium detectors. γ-ray energies and their time measured with respect to the rf pulse train were collected and a time-γ matrix was constructed and analyzed.

*Alison.Bruce@brighton.ac.uk
†Current address: Department of Physics & Astronomy, University of Kentucky, Lexington KY 40506, USA.
‡Current address: Department of Physics, University of York, Heslington, York YO10 5DD, UK.

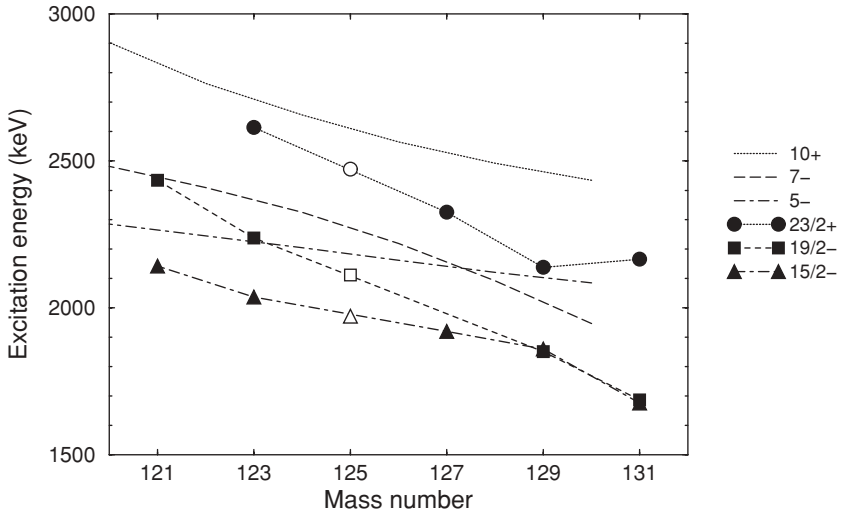

FIG. 1. Comparison of the $J^\pi = \frac{23}{2}^+$, $\frac{19}{2}^-$, and $\frac{15}{2}^-$ states in the odd-A antimony isotopes [1–5,7,8] with the energies of the $J^\pi = 10^+$, 7^-, and 5^- states in the even-A tin isotopes [9]. The J^π values for the levels in ^{125}Sb are uncertain and therefore are shown as open symbols.

III. EXPERIMENTAL RESULTS

A. ^{125}Sb

The level scheme for ^{125}Sb is shown in Fig. 2 and Table I lists the relative intensities of transitions below the isomeric states in ^{125}Sb, measured using the beam pulsing profile of 2 ns on/1.7 μs off with a condition requiring that the events were detected at least 100 ns after the beam pulse. Intensities are normalized to the 1090.0 keV transition. The half-lives of states at 1972, 2113, 2326, and 2472 keV were also obtained. Figure 3(a) shows the decay profile of the 2472 keV state, obtained by gating on the 146.3 keV transition. The straight line shows the fit to the decay curve, which gives the half-life of this state as 272(16) ns. Figure 3(b) shows the time spectrum obtained by gating on the 1067.8 keV transition. As the 1972 keV level is fed strongly by the 2113 keV state, which is itself isomeric, the spectrum shows a two-component decay and has been fitted using the value of 28.0(7) μs for the half-life of the 2113 keV state obtained from an analysis of the time profile of the 140.9 keV transition. This yields a half-life of 4.1(2) μs for the 1972 keV state which supersedes that quoted in Ref. [15] [5.7(3) μs]. This difference is due to a typographical error in the previous analysis.

The fifth column of Table I lists the conversion coefficients measured in this experiment. Preliminary results from this analysis have been published in Ref. [15]. Conversion coefficients could not be measured for the 105.1, 107.9, or 131.8 keV transitions because of the high level of background in the low-energy region of the electron spectrum. However, a value of α_{tot} has been deduced for the 131.8 keV transition from a balance of intensities across the 2194 keV state. The multipolarity of the 1104.2 keV transition that depopulates the 2194 keV level is not known but the energy of this transition is so high that the difference between the conversion coefficient for an $E1$ transition and an $E2$ transition is insignificant. The internal conversion coefficient of the 131.8 keV transition is consistent with it having a multipolarity of $E2$. The 140.9 keV transition is observed in the γ-ray spectrum as a doublet with a 139.7 keV contaminant transition and therefore these peaks had to be unfolded. For both the electrons and γ

TABLE I. γ-ray energies, initial and final level energies, relative γ-ray intensities, and conversion coefficients of transitions below the isomeric states in ^{125}Sb. The γ-ray energies have an uncertainty of $\pm$0.3 keV.

E_γ (keV)	E_i	E_f	I_γ	α_K	$\alpha_{K(\text{theory})}$ [14]	Assigned multipolarity
105.1	2217.9	2112.7	2.4(2)			
107.9	2325.9	2217.9	9.4(5)			
131.8	2325.9	2194.2	9.5(6)	0.58(4)[a]	$E2 = 0.62$[a]	$E2$
140.9	2112.7	1971.8	52.9(15)	0.51(6)	$E2 = 0.37$, $M3 = 8.83$	$E2$
146.3	2472.2	2325.9	30.8(4)	0.34(2)	$E2 = 0.33$	$E2$
246.1	2217.9	1971.8	8.3(3)	0.048(13)	$M1 = 0.045$	$M1$
331.5	2325.9	1994.4	17.2(8)	0.022(5)	$M1 = 0.021$, $E2 = 0.022$	$M1$ or $E2$
881.8	1971.8	1090.0	75.9(10)	0.0035(9)	$M2 = 0.0050$, $E3 = 0.0034$	$M2 + E3$ ($\delta^2 \geqslant 0.56$)
904.0	1971.8	1067.8	119(3)	0.0034(4)	$E3 = 0.0032$	$E3$
904.4	1994.4	1090.0	21.8(5)	0.0015(1)	$E2 = 0.0015$	$E2$
1067.8	1067.8	0.0	118.6(14)	0.0013(2)	$M1 = 0.0013$, $E2 = 0.0010$	$M1 + E2$ ($\delta^2 \leqslant 2.4$)
1090.0	1090.0	0.0	100.0(13)	0.0012(3)	$E2 = 0.0010$	$E2$
1104.2	2194.2	1090.0	15.0(4)			$E2$

[a]α_{tot} (see text for details).

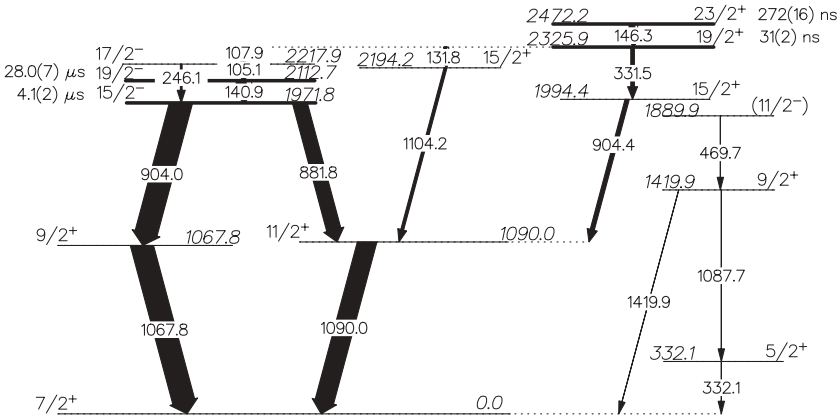

FIG. 2. Level scheme for ^{125}Sb from the present work. The γ-ray energies are given in keV and the thickness of the arrows represents the relative γ-ray intensity. The prompt 1419.9, 1087.7, 469.7, and 332.1 keV transitions are known from β-decay studies [13]; however, the intensities of these states were too weak to be measured in the current work.

rays, energy spectra were produced from the beam-γ matrix with gates 10–43 μs and 43–76 μs after the prompt peak. The number of counts making up the 139.7 and 140.9 keV peaks was determined for each time gate and put into a 2×2 matrix as a percentage of the total number of counts. This matrix was then transposed to give the coefficients needed to resolve the 139.7 and 140.9 keV γ-ray peaks from the time gated spectra. Figure 4 illustrates the results of this process and shows that the 139.7 keV contaminant was not seen in the electron spectrum, indicating that it was not from the target. The electron spectrum does not show any evidence for a peak corresponding to the 1104.2 keV transition and this nonobservation implies that the 1104.2 keV transition is of either $E1$ or $E2$ multipolarity.

The level scheme shown in Fig. 2 is based on that published by Liu *et al.* [7,8], discussed in Sec. I, but shows the half-lives measured in the current work. The J^π values assigned to the isomeric states in the current work are consistent with those assigned in Refs. [7,8] and, specifically, the spin and parity of the 2472 keV state is confirmed as $\frac{23}{2}^+$. This is not consistent with the value of $(\frac{19}{2}^-)$ assigned in the work of Porquet *et al.* [4] but the previous interpretation was based only on systematic arguments and so the assignment made in the current work is preferred. The 2326 keV state has been observed as isomeric in the current work and may not have been identified as such previously [4,7,8] because of the short half-life [31(2) ns], which may have been outside their experimental sensitivity.

B. ^{123}Sb

The experiment on ^{123}Sb provided evidence for an isomeric state with a half-life greater than 2 μs. The 2614 keV state was measured to have a half-life of 66(4) μs by fitting the summed γ-gated spectra shown in Fig. 5. In parallel with the current work, Jones *et al.* [5] have obtained a half-life of 52(3) μs for this state. The reason for the discrepancy between this value and that measured in the current work is unclear.

IV. DISCUSSION

Isotopes in the range ^{121}Sb to ^{131}Sb have 1 proton and 20–30 neutrons in the $Z/N = 50$–82 shell, which contains the $g_{\frac{7}{2}}$, $d_{\frac{5}{2}}$, $d_{\frac{3}{2}}$, $s_{\frac{1}{2}}$, and $h_{\frac{11}{2}}$ orbitals. The shell-model calculations presented in the current work were performed using the Oxbash code [16] and the SN100PN [17] interaction and model space. The single-particle energies used were deduced from the experimentally observed level schemes of ^{131}Sn [18] and ^{133}Sb [19]. This interaction has been used with good success to describe the excitation energies and magnetic moments of the even mass $^{124-130}$Sn, $^{130-134}$Te, and ^{134}Xe isotopes [17]. However, calculations in the full model space could only be achieved for odd-mass antimony nuclei heavier than ^{125}Sb; therefore, it was necessary to truncate the space. Examination

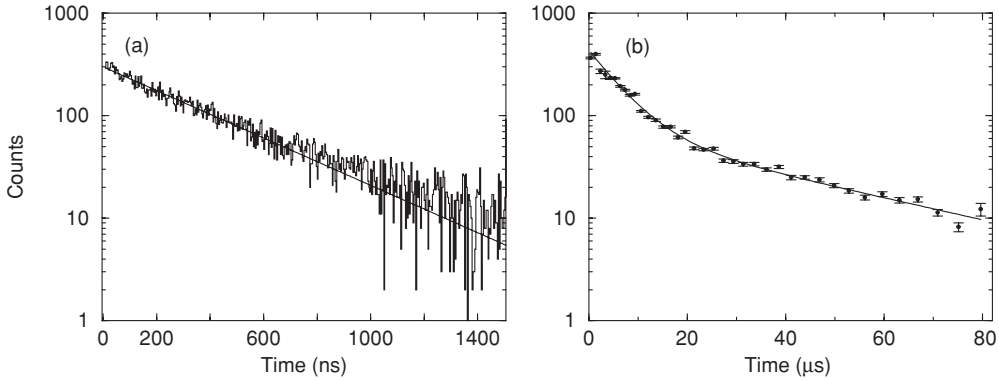

FIG. 3. (a) A single-component fit to the decay profile of the 146.3 keV transition de-exciting the 2472 keV state in ^{125}Sb. The straight line shows the fit to the data giving a half-life of 272(16) ns. (b) A two-component fit to the decay spectrum produced by gating on the 1067.8 keV transition in ^{125}Sb. Assuming a half-life of 28.0(7) μs for the 2113 keV level, the fit gives the half-life of the 1972 keV state as 4.1(2) μs.

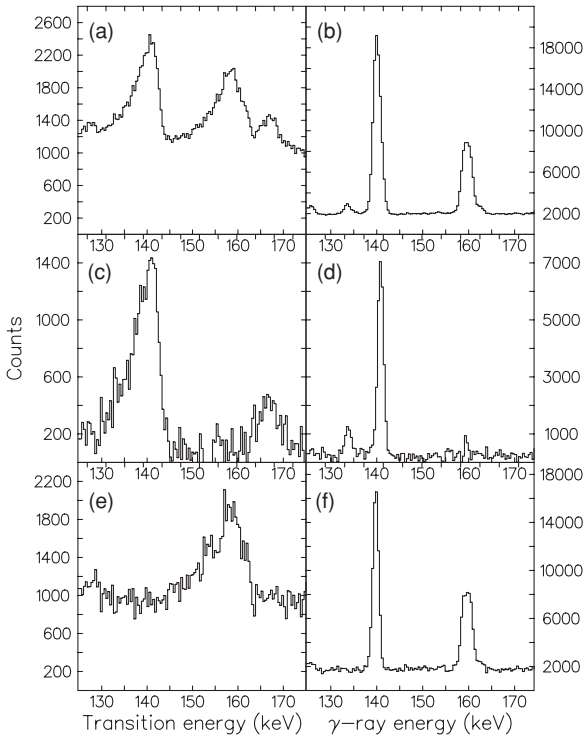

FIG. 4. Results of the unfolding of the 139.7/140.9 keV doublet for the electron and γ-ray spectra. Panels (a) and (b) are the raw electron and γ-ray spectra. Panels (c) and (d) show the unfolded 140.9 keV peaks from the transition in ^{125}Sb. Panels (e) and (f) show the unfolded 139.7 keV contaminant peak. Transition energies are calculated using the antimony K-shell binding energy of 30.5 keV.

of the wave functions calculated in the full space indicated that the following truncation would be appropriate:

(i) The odd proton was restricted to the $g_{\frac{7}{2}}$, $d_{\frac{5}{2}}$, and $d_{\frac{3}{2}}$ orbits.

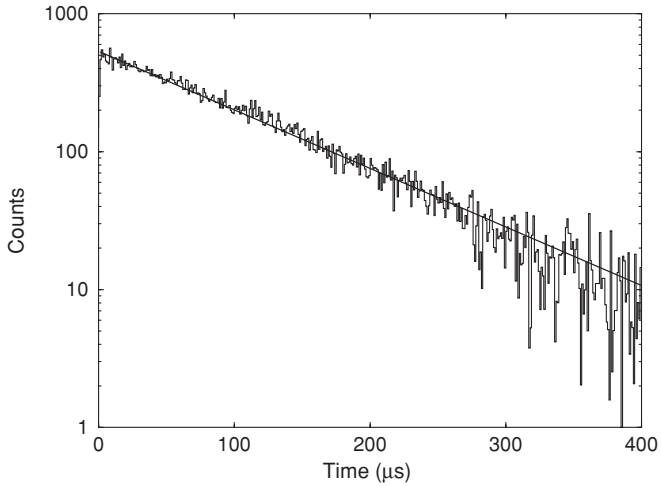

FIG. 5. Summed time spectrum obtained by gating on the 127.6, 442.0, 955.9, and 1088.7 keV transitions below the 2614 keV state in ^{123}Sb. The straight line shows the fit to the data, giving a half-life of 66(4) μs.

(ii) The $g_{\frac{7}{2}}$ neutron orbit was required to be full and the $d_{\frac{5}{2}}$ orbit was required to have a minimum occupancy of 4. The remaining neutrons (8 for ^{121}Sb and 18 for ^{131}Sb) were allowed to occupy the remainder of the $d_{\frac{5}{2}}$, $d_{\frac{3}{2}}$, $s_{\frac{1}{2}}$, and $h_{\frac{11}{2}}$ space.

A. Level energies

The calculated level energies are compressed in the restricted space. To compensate for this, multiplicative factors were derived by comparing the excitation energies of the first $J^\pi = \frac{9}{2}^+, \frac{11}{2}^+, \frac{15}{2}^+, \frac{15}{2}^-, \frac{19}{2}^+, \frac{19}{2}^-$, and $\frac{23}{2}^+$ states in ^{127,129,131}Sb calculated using the restricted model space with those calculated using the full model space. This gave compression factors of 1.19 for ^{131}Sb, 1.26 for ^{129}Sb, and 1.32 for ^{127}Sb. A linear extrapolation of these values gives a compression factor of 1.44 for ^{125}Sb. The calculated level scheme multiplied by this factor is shown in Fig. 6 with the arrows representing experimentally observed transitions. The overall level of agreement between the calculated levels shown in Fig. 6 and the experimental level scheme, shown in Fig. 2, is generally within ~200 keV but there are a few notable exceptions. The first $J^\pi = \frac{5}{2}^+$ state is calculated to be ~800 keV too high and the second $J^\pi = \frac{9}{2}^+$ state is calculated to be ~700 keV above the first, while experimentally it is only ~350 keV above.

Figure 7 shows the experimentally determined level energies for the isomeric $J^\pi = \frac{23}{2}^+, \frac{19}{2}^+, \frac{19}{2}^-$, and $\frac{15}{2}^-$ states as well as for the $J^\pi = \frac{5}{2}, \frac{9}{2}, \frac{11}{2}^+$, and $\frac{15}{2}^+$ states in ^{123}Sb taken from Refs. [4,5], in comparison with those calculated using the restricted model space and multiplied by the extrapolated factor of 1.52. The figure shows that the agreement between experiment and theory for these states is generally excellent, agreeing to within 100 keV. However, as in ^{125}Sb, the calculated energy of the $J^\pi = \frac{5}{2}^+$ state is several hundred keV higher than is observed experimentally and the second $J^\pi =$

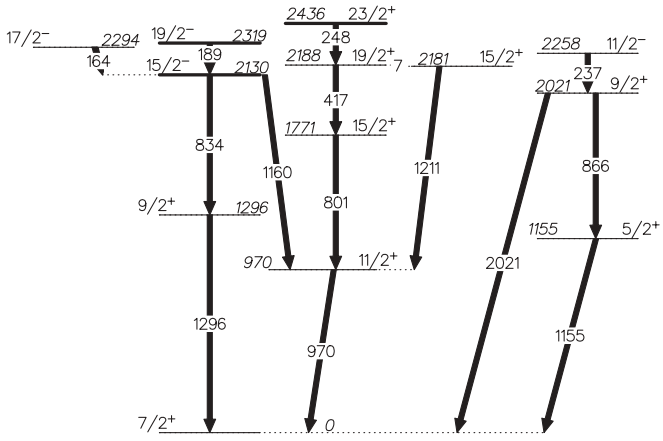

FIG. 6. Calculated level scheme for ^{125}Sb produced using the restricted SN100PN model space and showing only the levels that were experimentally observed in this work. Level energies were multiplied by a factor of 1.44 to account for the effect of the restricted model space. The width of the arrows does not represent the transition strengths.

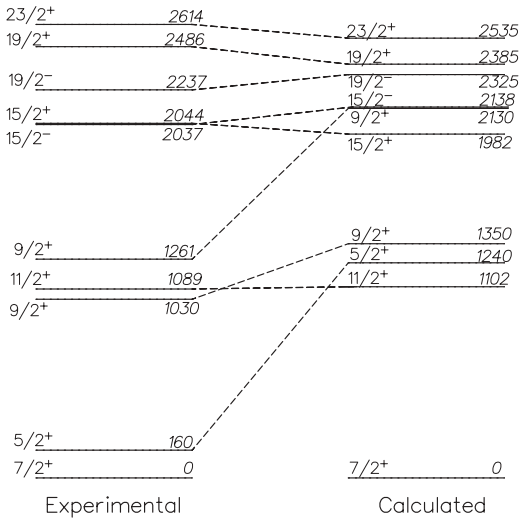

FIG. 7. A comparison of calculated and experimental level energies for ^{123}Sb showing selected levels below the 2614 keV isomer. Calculated level energies were multiplied by a factor of 1.52 to account for the effect of the restricted model space.

$\frac{9}{2}^+$ state is almost 1 MeV higher in the calculation than is seen experimentally.

The $J^\pi = \frac{5}{2}^+$ state in ^{127}Sb is observed experimentally at 491 keV [1]. The results of calculations performed for ^{127}Sb using the full model space predict this state to be at 894 keV and so the poor agreement between experiment and theory in the case of ^{125,123}Sb is not due to the restricted model space but possibly to the proton-neutron interaction used.

The first $J^\pi = \frac{9}{2}^+$ state in ^{121}Sb has been identified from (t,α) reaction studies at 935 keV [20] and has been explained as being generated by the excitation of a $g_{\frac{9}{2}}$ proton across the $Z = 50$ shell gap. The corresponding states in ^{123,125}Sb have been identified at 1324 and 1813 keV, respectively [20]. The second $J^\pi = \frac{9}{2}^+$ states in ^{123,125}Sb are therefore not due to this mode of excitation but are likely the result of collective core deformation effects that are not accounted for in the calculations.

B. Wave functions and transition probabilities

Examination of the calculated wave functions of the isomeric states indicates that the wave function of the $J^\pi = \frac{23}{2}^+$ isomer in ^{125}Sb can be expressed as $|\Psi_{\rm Sb}^{\frac{23}{2}^+}\rangle = \sim 74\%|\Psi_{\rm Sn}^{10^+}\rangle \otimes \pi g_{\frac{7}{2}}$, the wave function of the $J^\pi = \frac{19}{2}^+$ state populated by an $E2$ transition from the $J^\pi = \frac{23}{2}^+$ isomer can be expressed as $|\Psi_{\rm Sb}^{\frac{19}{2}^+}\rangle = \sim 70\%|\Psi_{\rm Sn}^{8^+}\rangle \otimes \pi g_{\frac{7}{2}}$, the wave function of the $J^\pi = \frac{19}{2}^-$ isomer can be expressed as $|\Psi_{\rm Sb}^{\frac{19}{2}^-}\rangle = \sim 80\%|\Psi_{\rm Sn}^{7^-}\rangle \otimes \pi g_{\frac{7}{2}}$, and the wave function of the $J^\pi = \frac{15}{2}^-$ isomers can be expressed as $|\Psi_{\rm Sb}^{\frac{15}{2}^-}\rangle = \sim 82\%|\Psi_{\rm Sn}^{5^-}\rangle \otimes \pi g_{\frac{7}{2}}$. Analysis of the wave functions of these states in ^{121,123,127,129}Sb and ^{120,122,126,128}Sn show comparable levels of overlap. This is consistent with the qualitative interpretation presented in the Introduction.

Table II summarizes the information on the transition probabilities for the decay from the isomeric states in ^{121}Sb to ^{131}Sb. Figure 8 shows these data in comparison with the analogous

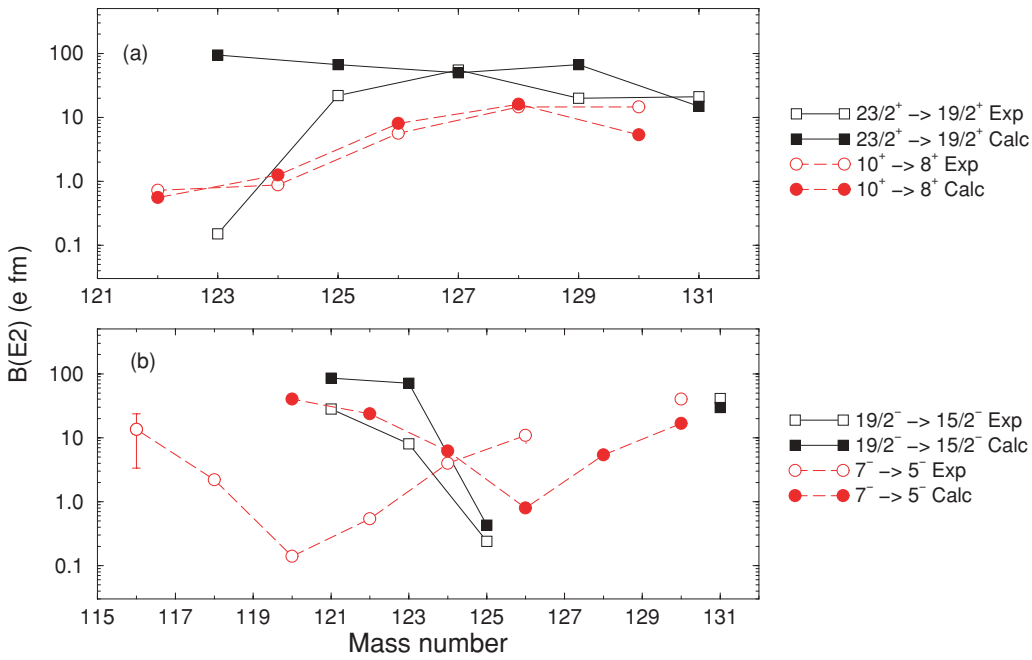

FIG. 8. (Color online) Calculated and experimentally observed transition probabilities as a function of mass number. (a) The $B(E2: \frac{23}{2}^+ \rightarrow \frac{19}{2}^+)$ values in the odd-A antimony isotopes plotted with the $B(E2: 10^+ \rightarrow 8^+)$ in the even-A tin isotopes. (b) The $B(E2: \frac{19}{2}^- \rightarrow \frac{15}{2}^-)$ values in the odd-A antimony isotopes plotted with the $B(E2: 7^- \rightarrow 5^-)$ in the even-A tin isotopes. Experimental errors are smaller than the size of the data points unless shown.

TABLE II. Experimentally determined reduced transition probabilities.

A	Level (keV)	$T_{\frac{1}{2}}$	Transition	E_γ (keV)	$\sigma\lambda$	$\alpha_{\text{tot (theory)}}$ [14]	γ-ray branching	Ref.	$B(\sigma\lambda)$ (e^2 fm$^{2\lambda}$ or μ_0^2 fm$^{2\lambda-2}$)
131	2166.3	1.1(2) μs	$\frac{23}{2}^+ \rightarrow \frac{19}{2}^+$	96.4	$E2$	1.88	100	[2]	21(4)
	1687.9	4.3(8) μs	$\frac{19}{2}^- \rightarrow \frac{15}{2}^-$	11.2	$E2$	1.82×10^4	100	[2]	41(8)
	1676.7	65(5) μs	$\frac{15}{2}^- \rightarrow \frac{9}{2}^+$	447.4	$E3$	3.21×10^{-2}	4[a]	[2,22]	201(15)
			$\frac{15}{2}^- \rightarrow \frac{11}{2}^+$	450.0	$M2$	3.87×10^{-2}	96[a]	[2,22]	$3.9(3) \times 10^{-2}$
129	2138.9	1.1(1) μs	$\frac{23}{2}^+ \rightarrow \frac{19}{2}^+$	98.6	$E2$	1.73	100	[3]	20(2)
	1851.0	17.7(1) min	$\frac{19}{2}^- \rightarrow \frac{11}{2}^+$	722.6	$M4$	5.47×10^{-2}	100	[23]	6140(35)
	1860.9	2.2(2) μs	$\frac{15}{2}^- \rightarrow \frac{19}{2}^-$	9.8	$E2$	3.56×10^4	88[a]	[3,23]	80(7)
			$\frac{15}{2}^- \rightarrow \frac{9}{2}^+$	699.6	$E3$	7.62×10^{-3}	8[a]	[3,23]	$1.7(2) \times 10^{-2}$
			$\frac{15}{2}^- \rightarrow \frac{11}{2}^+$	732.5	$M2$	9.51×10^{-3}	4[a]	[3,23]	$1.4(1) \times 10^{-7}$
127	2324.8	165(20) ns	$\frac{23}{2}^+ \rightarrow \frac{19}{2}^+$[b]	130.4	$E2$	6.44×10^{-1}	100	[4]	55(7)
	1920.2	11(1) μs	$\frac{15}{2}^- \rightarrow \frac{9}{2}^+$	805.9	$E3$	5.09×10^{-2}	58(8)	[1]	288(60)
			$\frac{15}{2}^- \rightarrow \frac{11}{2}^+$	824.7	$M2$	6.89×10^{-3}	42(10)	[1]	$5(1) \times 10^{-3}$
125	2472.2	272(16) ns	$\frac{23}{2}^+ \rightarrow \frac{19}{2}^+$	146.3	$E2$	4.29×10^{-1}	100	[c]	22(1)
	2325.9	31(2) ns	$\frac{19}{2}^+ \rightarrow \frac{15}{2}^+_1$	331.5	$E2$	2.68×10^{-2}	48(3)	[c]	1.8(2)
			$\frac{19}{2}^+ \rightarrow \frac{15}{2}^+_2$	131.8	$E2$	6.20×10^{-1}	26(2)	[c]	98(11)
			$\frac{19}{2}^+ \rightarrow \frac{17}{2}^-$	107.9	$E1$	1.52×10^{-1}	26(2)	[c]	$2.4(3) \times 10^{-6}$
	2112.7	28.0(7) μs	$\frac{19}{2}^- \rightarrow \frac{15}{2}^-$	140.9	$E2$	4.90×10^{-1}	100	[c]	$2.4(1) \times 10^{-1}$
	1971.8	4.1(2) μs	$\frac{15}{2}^- \rightarrow \frac{11}{2}^+$	881.8	$E3$[d]	$4.6(6) \times 10^{-3}$	39(1)	[c]	188(90)
			$\frac{15}{2}^- \rightarrow \frac{9}{2}^+$	904.0	$E3$	3.72×10^{-3}	61(2)	[c]	365(29)
123	2614.1	66(4) μs	$\frac{23}{2}^+ \rightarrow \frac{19}{2}^+$	127.6	$E2$	6.95×10^{-1}	100	[c]	$1.5(1) \times 10^{-1}$
	2486.3	7.9(4) ns	$\frac{19}{2}^+ \rightarrow \frac{15}{2}^+$	441.9	$E2$	1.11×10^{-2}	100	[5]	4.2(2)
	2239.1	190(30) ns	$\frac{19}{2}^- \rightarrow \frac{15}{2}^-$	201.0	$E2$	1.42×10^{-1}	100	[5]	8.0(1)
	2038.2	37(4) ns	$\frac{15}{2}^- \rightarrow \frac{11}{2}^-$	381.7	$E2$	1.73×10^{-2}	100	[5]	1.9(2)
121	2434.3	8.5(5) ns	$\frac{19}{2}^- \rightarrow \frac{15}{2}^-$	292.3	$E2$	4.03×10^{-2}	94(1)	[5]	28(2)
			$\frac{19}{2}^- \rightarrow \frac{17}{2}^+$	77.9	$E1$[e]	3.81×10^{-1}	6(1)	[5]	$6(1) \times 10^{-6}$

[a] No errors are quoted in the original publication.
[b] The states at 2325 and 2194 keV were assigned $J^\pi = \frac{19}{2}^-$ and $\frac{15}{2}^-$ in Ref. [4] but are interpreted in the current work as the $J^\pi = \frac{23}{2}^+$ and $\frac{19}{2}^+$ states.
[c] This work.
[d] $E3$ component of the mixed $M2 + E3$ transition, calculated using the δ^2 value listed in Table I.
[e] Assuming a pure $E1$ transition.

transitions in the neighboring even-A tin isotopes and with the results of the shell-model calculations using standard effective charges of $e_p = 1.5$ and $e_n = 0.5$. The values calculated for ^{129,131}Sb in the restricted space are in excellent agreement with those obtained from the unrestricted calculations giving further faith in the validity of the approximation.

Figure 8(a) shows that the calculated values for the $B(E2 : \frac{23}{2}^+ \rightarrow \frac{19}{2}^+)$ (closed squares) agree with the data (open squares) to within a factor of three for $A > 125$ but do not reproduce the rapid drop (approximately two orders of magnitude) between ^{125}Sb and ^{123}Sb. It is of note that the experimental data have the same shape as for the $B(E2 : 10^+ \rightarrow 8^+)$ values in the neighboring even-A tin isotopes (circles). The $J^\pi = 10^+$ and 8^+ states in the even-A tin isotopes and the $\frac{23}{2}^+$ and $\frac{19}{2}^+$ states in the odd-A antimony isotopes have $h_{\frac{11}{2}}$ neutron configurations. Inspection of the level schemes shows that the $J^\pi = 10^+ \rightarrow 8^+$ and $\frac{23}{2}^+ \rightarrow \frac{19}{2}^+$ transitions proceed between states of the same seniority. Because the $B(E2)$ values of these transitions depend critically on the occupation number of the $h_{\frac{11}{2}}$ orbital, a dependence on A is expected. In particular, at the point of half-filling, the particle and hole contributions are equal and so the $B(E2)$ value reduces to zero [21]. The experimental trend shown in Fig. 8(a) for $121 \leqslant A \leqslant 124$ can therefore be attributed to the half-filling of the $h_{\frac{11}{2}}$ neutron orbital at $N \sim 73$.

Figure 8(b) shows the $B(E2: \frac{19}{2}^- \rightarrow \frac{15}{2}^-)$ values in antimony (squares) alongside the $B(E2: 7^- \rightarrow 5^-)$ values in tin (circles). No values are shown for ^{129}Sb as the $J^\pi = \frac{19}{2}^-$ state is not observed to decay to the $\frac{15}{2}^-$ state. The state assigned $J^\pi = \frac{19}{2}^-$ in ^{127}Sb by Porquet *et al.* [4] is interpreted as the $J^\pi = \frac{23}{2}^+$ state in the current work. No other $J^\pi = \frac{19}{2}^-$ states are known in ^{127}Sb and so no $B(E2: \frac{19}{2}^- \rightarrow \frac{15}{2}^-)$ value is given for ^{127}Sb. The calculations for antimony (closed squares) clearly reproduce the systematics of the experimental values, in particular the reduction by two orders of magnitude between $A = 121$ and 125 and the increase of the same magnitude between $A = 125$ and 131. They overestimate the transition probabilities for ^{121,123}Sb by only a factor of $\sim$8. It is interesting to note that the experimental values for $B(E2: 7^- \rightarrow 5^-)$ (open circles) show the same shape as the values for $B(E2: \frac{19}{2}^- \rightarrow \frac{15}{2}^-)$ (open squares) but with a shift of $\sim$6 mass units. The calculated $B(E2: 7^- \rightarrow 5^-)$ values (closed circles) do not reproduce this and indeed overlap with the values for $B(E2: \frac{19}{2}^- \rightarrow \frac{15}{2}^-)$ (squares). This indicates that the calculated wave functions for the isomeric $J^\pi = 7^-$ and $J^\pi = 5^-$ states in the even-A tin isotopes do not reflect the experimental ones. This is not related to the truncated model space as calculations for the tin isotopes performed using the full model space show the same trend. The results for the odd-A antimony isotopes show that the addition of a single proton enables the calculated wave functions to reflect the experimental wave functions with much greater success. The origin of this anomaly is not clear. However, the underlying feature is that the $B(E2)$ data for the $J^\pi = \frac{19}{2}^-$ and $J^\pi = \frac{15}{2}^-$ states do not support the interpretation of the states in antimony being generated by the simple coupling of the extra proton to the $J^\pi = 7^-$ and $J^\pi = 5^-$ isomeric states in the tin core, implied by the energy systematics shown in Fig. 1.

V. CONCLUSIONS

The half-lives of excited states in ^{123,125}Sb have been measured and the J^π values of excited states in ^{125}Sb have been confirmed. The range of nuclei for which Oxbash calculations can be performed has been extended down to ^{121}Sb by the choice of a suitable truncation of the $N/Z = 50$–82 model space. A comparison of the systematics of the energy levels and of the transition probabilities with those of neighboring nuclei and with the results of shell-model calculations casts doubt on the previous interpretation of the negative parity isomeric states in antimony nuclei as an odd proton coupled to isomeric structures in neighboring even-A tin nuclei.

ACKNOWLEDGMENTS

The visitors to the ANU thank the technical and academic staff of the 14UD accelerator at the Australian National University for their assistance and hospitality. V. Pucknell at STFC Daresbury Laboratory is thanked for his help in running the shell-model calculations. D.S.J. and J.N.O. acknowledge receipt of EPSRC postgraduate grants. This work has been performed under an ANU-EPSRC agreement.

[1] K. E. Apt and W. B. Walters, Phys. Rev. C **9**, 310 (1974).
[2] J. Genevey *et al.*, Eur. Phys. J. A **9**, 191 (2000).
[3] J. Genevey *et al.*, Phys. Rev. C **67**, 054312 (2003).
[4] M.-G. Porquet *et al.*, Eur. Phys. J. A **24**, 39 (2005).
[5] G. A. Jones *et al.*, AIP Conf. Proc. **853**, 342 (2006) and (private communications).
[6] J. N. Orce, Ph.D. thesis, University of Brighton (unpublished, 2003).
[7] Z. Liu *et al.*, High Energy Phys. Nucl. Phys. **26**, 1195 (2002).
[8] Z. Liu *et al.*, Sci. China Ser. G **46**, 390 (2003).
[9] R. B. Firestone, *Table of Isotopes,* 8th ed. (Wiley & Sons, New York, 1996).
[10] T. Kibédi *et al.*, Astrophys. J. **489**, 951 (1997).
[11] T. Kibédi *et al.*, Nucl. Instrum. Methods Phys. Res. A **294**, 523 (1990).
[12] G. D. Dracoulis and A. P. Byrne, ANU-P/1052 (unpublished), 1995, p. 115.
[13] S. H. Devare and H. G. Devare, Phys. Rev. **133**, B568 (1964).
[14] T. Kibédi *et al.*, AIP Conf. Proc. **769**, 268 (2005).
[15] D. S. Judson *et al.*, J. Phys. G: Nucl. Part. Phys. **31**, S1899 (2005).
[16] B. A. Brown *et al.*, Oxbash for Windows, MSU-NSCL Report 1289.
[17] B. A. Brown, N. J. Stone, J. R. Stone, I. S. Towner, and M. Hjorth-Jensen, Phys. Rev. C **71**, 044317 (2005).
[18] B. Fogelberg, H. Gausemel, K. A. Mezilev, P. Hoff, H. Mach, M. Sanchez-Vega, A. Lindroth, E. Ramstrom, J. Genevey, J. A. Pinston, and M. Rejmund, Phys. Rev. C **70**, 034312 (2004).
[19] M. Sanchez-Vega, B. Fogelberg, H. Mach, R. B. E. Taylor, A. Lindroth, and J. Blomqvist, Phys. Rev. Lett. **80**, 5504 (1998).
[20] M. Conjeaud *et al.*, Nucl. Phys. **A215**, 383 (1973).
[21] R. Broda *et al.*, Phys. Rev. Lett. **68**, 1671 (1992).
[22] C. A. Stone *et al.*, in Proc. 5th Int. Conf. Nuclei Far from Stability, Rosseau Lake, Canada 1987 (1988), p. 429.
[23] C. A. Stone and W. B. Walters, Z. Phys. A **328**, 257 (1987).